THE JOURNAL OF PHYSICAL CHEMISTRY C

ARTICLE

pubs.acs.org/JPCC

Synthesis and Characterization of Organically Soluble Cu-Doped ZnS Nanocrystals with Br Co-activator

Carley Corrado,[†] Jason K. Cooper,[†] Morgan Hawker,[†] Jenny Hensel,[†] Grant Livingston,[†] Sheraz Gul,[†] Brian Vollbrecht,[‡] Frank Bridges,[‡] and Jin Z. Zhang*[,†]

[†]Department of Chemistry and Biochemistry, University of California, Santa Cruz, California 95064, United States

[‡]Department of Physics, University of California, Santa Cruz, California 95064, United States

Supporting Information

ABSTRACT: Fluorescent, organically soluble Cu and Br codoped ZnS nanocrystals (NCs) were synthesized and characterized for the potential application of AC electroluminescent (EL) lighting devices. The doped NCs were optically characterized using UV−vis, photoluminescence (PL), Fourier transform infrared (FTIR), and time-resolved PL spectroscopy, and structurally characterized using transmission electron microscopy (TEM) and extended X-ray absorption fine structure (EXAFS). The PL emission of the undoped ZnS NCs upon λ_{ex} = 280 nm was broad with a peak in the range of 450−470 nm, depending on the preparation of the NCs. Upon doping ZnS NCs with Cu, the PL emission was increased slightly with little change in spectral features. When Br dopant was added in addition to Cu, the codoped ZnS NCs showed much stronger PL emission (∼5 ×) compared to the undoped or Cu-doped sample. In conjunction with time-resolved PL results, this enhanced emission is attributed to a donor−acceptor (D−A) type of transition, between the Br electron trap and Cu hole trap, respectively. The time-resolved PL studies provide important information about the lifetimes of associated states and help to gain new insights into the nature of the states involved in the observed PL. The EXAFS data reveal that Br is clearly incorporated into the NCs. Increased disorder around Br with increasing Cu suggests that the Br is located near Cu within the ZnS lattice. This study demonstrates successful Cu-doping of ZnS NCs by using a halogen coactivator, for the first time, in an organic solvent. Organic soluble systems have proven more advantageous for preparation of high-quality thin films.

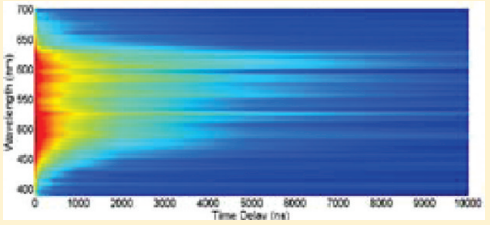

1. INTRODUCTION

Doped semiconductor nanocrystals (NCs) make up an important subset of nanomaterials where a small percentage of intentionally added impurities, called dopants, are introduced into NCs altering their electrical, magnetic, and optical properties for a wide range of applications.[1−12] One of these that has recently been a growing area of research is in developing alternating current-driven electroluminescent (EL) devices for next-generation high efficiency lighting technology that utilizes NCs as the phosphor material.[13−21] They also afford advantages in fabrication of lighting devices due to their small size and variable composition allowing their emission to be finely tuned to emit at a desired wavelength over a broad spectral range.

ZnS is an attractive choice as a host material for doping and is the most common and widely studied phosphor material[22] because it is stable, inexpensive, and relatively nontoxic when compared to other NCs such as CdSe. ZnS has been "activated" or doped with a variety of metals including Mn, Cu, and Ag[1,8,23−32] that introduce an intermediate energy state within the bandgap, altering the wavelength of emission and the photophysical relaxation processes of the carriers in the host. Tuning the intermediate state allows for control of the emission wavelength within the visible and IR spectrum. Bulk ZnS doped with Cu (ZnS:Cu) has been widely used as a commercial phosphor material.[33] There is significant interest in making this material on the nanoscale regime because of the tunable emission and the potential to make ultrathin film devices. The benefit of making thinner devices is their lower turn-on voltage to achieve an equivalent electric field within the material.[15,34] ZnS:Cu NCs can be challenging to synthesize due to the difference in solubility of CuS and ZnS, their K_{sp} values being 2.5×10^{-48} and 2.2×10^{-22}, respectively, making their coprecipitation difficult. Even so, a variety of synthetic methods have been devised, including aqueous precipitation,[25,28,35−37] hydrothermal microemulsion route,[38] in polymeric networks,[39] and thermolysis of metal oleate complexes,[23] to mention a few. The majority of successful Cu-doping has occurred in aqueous systems. However, organically soluble NCs are desired for the fabrication of high quality thin-films.

Inclusion of a coactivator (or codopant) such as a halogen is one approach to increase the solubility of Cu in the ZnS host lattice as well as increase the D−A emission for making efficient EL phosphor materials.[26,40−44] Coactivators play an important role in the emission process by introducing a shallow donor state ∼0.25 eV[69] below the conduction band of the host forming a

Received: March 23, 2011
Revised: May 25, 2011
Published: June 23, 2011

luminescent center for donor−acceptor (D−A) pair luminescence emission. The radiative recombination process can thereby take place more efficiently between the codopant and dopant within the bandgap of the host material by reducing nonradiative relaxation pathways.[46−49] Though this approach has been used widely for synthesizing EL bulk phosphor materials, there have been few reports using this strategy for making nanophosphors.[25,28] Chlorine is the most common codopant used in bulk ZnS:Cu,Cl[33] even though phosphors made with Br as a codopant have been shown to be more efficient and resistant to deterioration.[40−42,50] This could partially be due to synthetic methods involving costly and difficult practices associated with firing the phosphors in hazardous HBr and H_2S gases in fixed ratio that is difficult to reproduce and cumbersome. An alternative synthetic route was devised by Chander, but there has been little research activity since.[42]

Combining earlier work on EL phosphor optimization using codoping with the newer field of doping NCs is an avenue that shows great promise for development of materials with tunable, intense, and stable emission in the visible and IR spectrum. Advances in new characterization techniques, e.g., high-resolution transmission electron microscopy (HRTEM) and extended X-ray absorption fine structure (EXAFS), make it possible to gain deep insight into the detailed structures of NCs at the atomic scale to correlate with their electronic energy levels and optical properties.

In this work, highly fluorescent and stable Cu-doped ZnS NCs are synthesized by addition of Br as a codopant in a nonpolar medium for the first time. Structural and optical properties of the pristine and codoped ZnS NCs have been systematically characterized using a combination of microscopy, X-ray, and spectroscopic techniques including TEM, EXAFS, ultaviolet−visible (UV−vis), photoluminescence (PL), Fourier transform infrared (FTIR), and time-resolved PL. Synergistic effects of codoping in the ZnS host NCs has been found in terms of significantly enhanced PL, which is important for potential optoelectronics applications. A model to explain the observed PL emission intensity enhancement and the role of the dopants is proposed and discussed.

2. EXPERIMENTAL SECTION

2.1. Materials. All the chemicals were of reagent grade, except zinc stearate, and used without further purification. Zinc stearate ($Zn(C_{18}H_{35}O_2)_2$, 557−05−1, tech. grade) was purchased from Sigma-Aldrich. Copper chloride dihydrate ($CuCl_2 \cdot 2H_2O$, 10125−13−0, 99+%) was purchased from Aldrich Chemical Co. 1-Hexadecanethiol ($CH_3(CH_2)_{15}SH$, 2917-26-2, 97%) was purchased from Alfa Aeser. Trioctylamine (TOA, 1116-76-3, 98%) and tetraoctylammonium bromide (TOAB, 14866-33-2) were purchased from Sigma Chemical Co. Oleic Acid (112-80-1) was purchased from Fisher Science Education. Methanol (67-56-1, 99.9%) and toluene (108−88−3, 99.9%) were both purchased from Fisher Scientific.

2.2. Synthesis of ZnS NCs. ZnS:Cu,Br NCs were synthesized by a method similar to that of Ehlert.[23] In a typical synthesis of ZnS:Cu,Br (0.8%) NCs, doped with 0.8 mol % Cu compared to Zn, the following reagents were mixed with a magnetic stir bar in a three-neck 50 mL round-bottomed flask: 8 mL of TOA, 0.0948 g (150 μmol) of zinc stearate, 40 μL of 0.03 M $CuCl_2 \cdot 2H_2O$ dissolved in oleic acid, 66 μL of oleic acid, and 50 μL of 0.075 M TOAB in TOA. The reaction mix was purged with Ar for 30 min and degassed to 200 mmHg three times to ensure an oxygen-free environment. The reaction mix was then heated to 80 °C under Ar, and 0.207 g (1.6 mmol) of 1-hexadecanethiol in 1 mL of TOA (prepared in a N_2(g) glovebox and kept air-free) was injected. The reaction temperature was then raised to 280 ± 5 °C and heated for 1 h. Next, the reaction was cooled to room temperature and then exposed to air for the cleaning procedure. The NCs were cleaned immediately after synthesis due to their decrease in PL if left in solution with the crude reaction mix.

2.3. Cleaning of ZnS NCs. The NCs were precipitated from solution by adding a mixture of toluene and methanol. The following 3 mL solutions of toluene and methanol were added sequentially with mixing in-between: 5:1, 2:1, 1:1, 1:2, and then 1:5. If the final 3 mL solution of toluene:methanol did not precipitate out the NCs entirely, additional 1:5 toluene to methanol solution was added. If the methanol became immiscible with the reaction mixture, additional toluene was slowly added. The cloudy, precipitated solution was then centrifuged at 3000 rpm for 20 min at room temperature and after, the supernatant was discarded. The NCs were washed and centrifuged again with 5 mL of 1:1 toluene to methanol. The "cleaned" NCs were then redispersed in hexane for analysis.

2.4. Instrumentation. Low-resolution TEM measurements were performed on a JEOL model JEM-1200EX microscope. High-resolution HRTEM measurements were performed on a Philips CM300-FEG at the National Center for Electron Microscopy at Lawrence Berkeley National Laboratory. The UV−vis absorption spectra were taken on a Hewlett-Packard 8452A diode array spectrophotometer at room temperature. The PL and PL excitation (PLE) spectra were measured on a Perkin-Elmer Luminescence Spectrometer LS50B at room temperature. Optical measurements were done with samples dissolved in hexanes. Centrifugation was performed on a Sorvall Legend RT. FTIR measurements were carried out with a Perkin-Elmer FTIR spectrometer (spectral resolution 4 cm^{-1}).

Time resolved PL measurements were collected on the NC suspension in hexane which had an optical density (OD) between 0.06 to 0.1 held in a 2 mm path length quartz fluorescence cuvette. The sample was pumped with the third harmonic (355 nm) of a Q-switched Nd:YAG laser (QuantaRay DCR-2) with pulse duration of 7 ns and power of 100 $\mu J\ mm^{-2}$. The excitation light was passed through a 1 mm slit before entering the cuvette. Collection of the emitted radiation was performed 90° to the excitation light by first passing it through a cutoff filter to remove scattered laser light (Schott OG-370). It was than separated with a spectrograph (Jarrel-Ash MonoSpec 27: holographic grating 150 grooves/mm) with entrance slit of 500 μm. Detection of the PL spectrum was performed with an intensified charge-coupled device (ICCD) (Andor DH520) whose intensifier photocathode had an extended red S-20 response and whose spectral response was recorded from 193 to 825 nm over 1024 channels.

The time-dependent PL intensity was first measured on the undoped ZnS sample by using a series of intensifier gate widths due to the low PL emission of the sample. The ZnS:Cu and ZnS:Cu,Br samples were characterized by using a series of fixed intensifier gate widths, but with varying the gate delay with respect to the excitation pulse. The gate width and delay times were controlled with a Stanford Research Systems DG-535 digital delay generator. In the former method, the beginning of the gate width was set to 20 ns after the peak of the excitation pulse measured with a scattering sample. The gate widths were 50, 200, 500, 1000, 5000, and 10 000 ns. The second method was collected by using a fixed gate width of 50 ns, and the delay times were 40, 140,

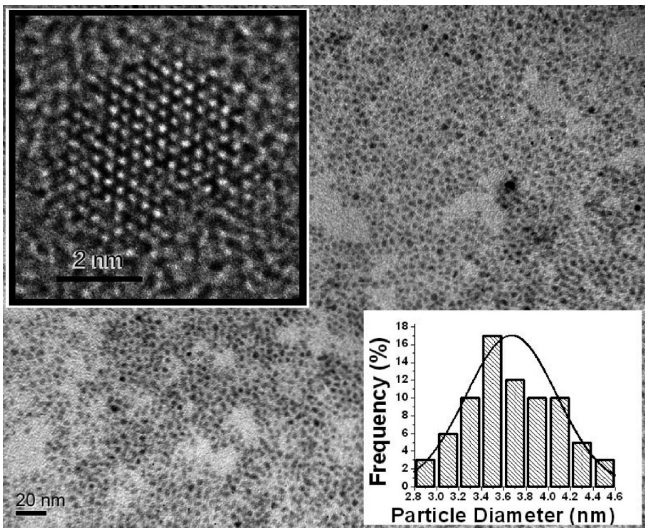

Figure 1. TEM of ZnS:Cu,Br NCs; the scale bar is 20 nm. The upper inset shows the HRTEM of a single NC. The lower inset shows a histogram of the particle size distribution.

240, 540, and 1020 ns. It was then fixed at 200 ns, and intensities were recorded at delays of 2085, 5085, and 10 085 ns; finally, the gate was fixed at 1000 ns, and delays of 10 495, 20 495, and 50 495 ns were collected. Spectra were further filtered with a box average of 10 points to remove shot noise.

Cu and Br fluorescence EXAFS data were collected on beamline 10−2 at Stanford Synchrotron Radiation Lightsource (SSRL) for several ZnS:Cu,Br NCs samples with Cu concentrations ranging from 0 to 0.8%. For the EXAFS samples, the NCs were deposited on filter paper and encapsulated with tape. The Si (111) double monochromator was detuned 50% to reduce harmonics, and the vertical slits were set at 0.7 mm, providing an energy resolution of 3 eV at the Br K-edge. All data were collected at 10 K to eliminate thermal vibrations. The Br concentration was measured for three of the samples by the ratio of the step heights at the Br and Zn K-edges (in transmission mode); 1.2% Br for the 0.8% Cu sample, 2% for the 0.04% Cu sample, and 1% Br for the 0.04% Cu sample. Since the relative Br fluorescence signal intensity was comparable for most of the samples, the Br concentration of the sample with no Cu must be similar ∼1%.

3. RESULTS

3.1. TEM and EXAFS Measurement. A representative TEM image of ZnS:Cu NCs is shown in Figure 1. The inset shows the HRTEM image of a single NC, which indicates high crystallinity. The average size of the ZnS:Cu,Br (0.8%) NCs after 1 h of reaction time was found to be 4 nm with a 12% size distribution.

EXAFS data was used to gain an understanding of the local structure of the Br-dopant within the ZnS lattice. An example of the *k*-space EXAFS data with Cu concentration of 0.8% is shown in Figure S1 of the Supporting Information. The data are high quality for *k*-space equal to about 10 $Å^{-1}$ but quickly become noisy for higher *k*; consequently, we limited the upper end of the transform window for the fast Fourier transforms (FFT) to 9.5 $Å^{-1}$. The *k*-space data for other samples were similar. These *k*-space data were FFT to *r*-space using an FFT range of 3.5−9.5 $Å^{-1}$.

In Figure 2 we show the *r*-space data (red online) for three samples with nominal concentrations from top to bottom: 0.8%,

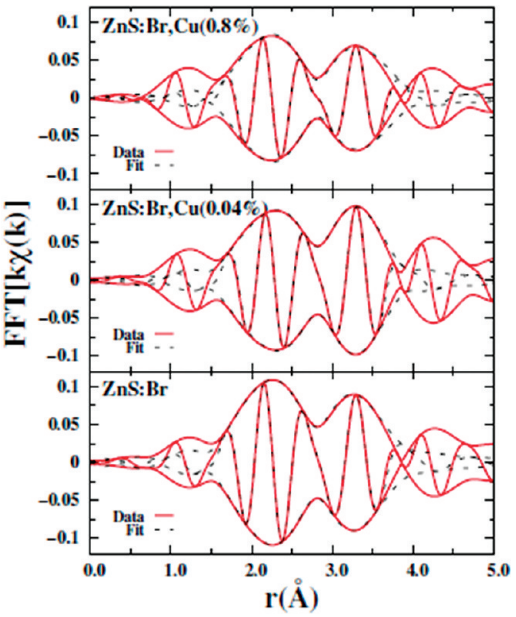

Figure 2. The *r*-space data (red solid line) at the Br K-edge, for ZnS:Cu, Br; from top to bottom, 0.8% Cu, 0.4% Cu, and no Cu. The Fourier transform range is 4−9.5 $Å^{-1}$ and the fast oscillation is the real part of the transform. The data were fit over the range 1.6−3.5 Å, to a sum of two peaks (Br−Zn and Br−S), and are shown as dashed lines.

0.04%, and 0%; each plot is the average of three scans. The plots clearly show that three similar peaks are present out to 4 Å. This means that there are at least three shells of neighbors about Br that are reasonably well ordered. The first two shells with peaks near 2.3 and 3.3 Å in Figure 2 correspond to Br−Zn and Br−S. The small peak near 1 Å is not an EXAFS peak (too short a distance) and is likely a result of atomic EXAFS[51] or multielectron excitations.[51,52] Surprisingly, however, the overall amplitude is much lower than expected, by at least a factor of 2, and smallest for the 0.8% sample.

To quantify the amplitude results and determine the pair distances for Br−Zn and Br−S, we calculated theoretical EXAFS functions for the Br−Zn and Br−S pairs using the program FEFF8[53] and the cubic zinc blende structure, and then fit each data scan to a sum of these two functions over the *r*-range 1.8−3.6 Å. Fits to the averaged data are shown in Figure 2 by dashed lines. The fit is excellent over this range. In these fits we allowed the two distances to vary and the widths, σ, to vary. In some fits we allowed the two amplitudes to vary independently; the amplitude ratio was close to 1:3 for each sample (varied from 1:2.8 to 1:3). Because a ratio of 1:3 is expected for the Br on a S site in ZnS, the ratio was held at 1:3. The Br−Zn peak amplitude for the 0.8% sample corresponds to about 1 Zn (and 3 S) neighbor, while for the ZnS:Br sample (no Cu) the peak amplitude corresponds to nearly two Zn (and 5−6 S) neighbors. σ for the Br−Zn peak varied from 0.073 to 0.091 Å while that for the Br−S peak was slightly larger (0.090−0.110 Å). Also note that one cannot force a significantly higher amplitude, the quality of the fits decreases rapidly if the amplitude differs by more than 15% from the best fit.

The distances for the first Br−Zn peak differs substantially from the S−Zn distance in ZnS: it is 0.11−0.13 Å longer, while the Br−S peak is slightly shorter by ∼0.04 Å. The significant

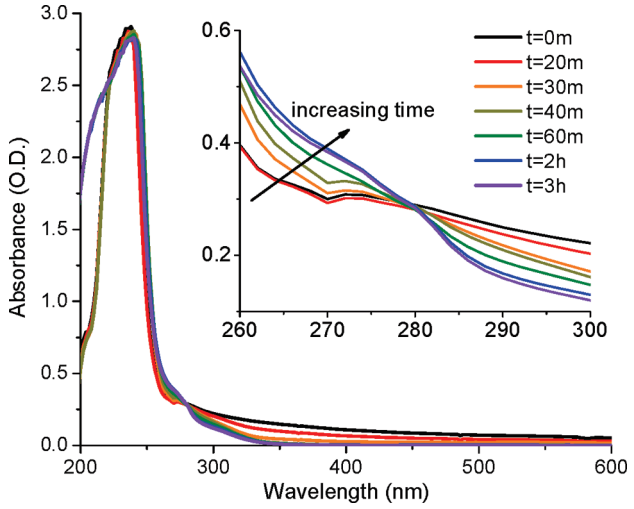

Figure 3. The UV−vis spectra of the ZnS:Cu,Br NCs aliquots taken during the synthesis after 0 min, 20 min, 30 min, 40 min, 60 min, 2 h, and 3 h.

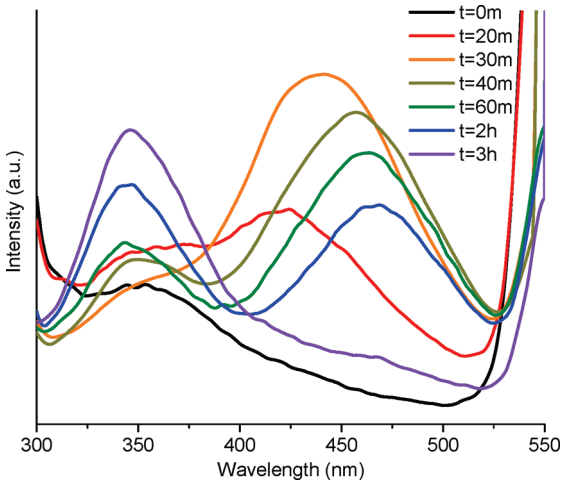

Figure 4. The PL emission spectra of ZnS:Cu,Br NCs aliquots with λ_{ex} = 280 nm taken during the synthesis after 0 min, 20 min, 30 min, 40 min, 60 min, 2 h, and 3 h.

increase in the Br−Zn distance can be understood from the fact that the Br^- ion is about 0.12 Å larger than the S^{2-} ion. Thus Br introduces substantial strain into the ZnS lattice.

3.2. UV−Vis Absorption and Static PL Characterization. The UV−vis electronic absorption spectra from 200 to 800 nm are shown in Figure 3. The spectra correspond to ZnS:Cu,Br NCs dispersed in hexane with reaction time from 0 to 3 h including t = 0 min being the time at which the reaction temperature reached 280 °C, as well as after 20 min, 30 min, 40 min, 60 min, 2 h, and 3 h. The isosbestic point occurs due to the concentration of each sample being adjusted to have an absorbance of 0.28 OD at the excitation wavelength of 280 nm to allow for quantitative comparison of PL emission intensity. The t = 0 min sample exhibits an apparent strong peak around 240 nm and a small peak around 275 nm. The peak near 240 nm is an artifact due to the decrease in instrumental response since the real absorption is expected to continue to increase toward shorter wavelength. The absorbance tail of the sample beyond the peak at 275 nm appears to continue toward longer wavelengths, an effect caused by scattering in the cloudy sample. This was also present to a lesser degree in the t = 20 min and t = 30 min samples and became less significant as the aliquots became less cloudy with reaction time. As the reaction time increased, the peak around 275 nm is red-shifted, as shown in the inset. This red-shift was attributed to an increase in size of the NCs. Since the Bohr exciton radius of ZnS is 2.2 nm and the diameter of the NCs is ∼4 nm, the quantum confinement effect is expected to be weak in the size range studied. The UV−vis evolution with reaction time shows no significant differences between the undoped samples and the codoped samples, data not shown.

Figure 4 shows the PL emission spectra in the range of 300−550 nm of ZnS:Cu,Br (0.8%) NCs excited by λ_{ex} = 280 nm with reaction time from 0 to 3 h of the crude reaction mix. The PL emission of the t = 0 min sample exhibits a broad band from 300 to 500 nm with a peak around 350 nm. The peak around 350 nm can be attributed to emission from the band edge (BE) of ZnS, or from shallow trap states very near the BE. The PL emission in the 400−500 nm region is apparently from deep trap states (DTS) due to a large red (Stokes) shift with respect to the BE position. There is an apparent emergence of a peak in each spectra starting at ∼525 nm, which is an artifact resulting from the Rayleigh scattering of the excitation light (λ_{ex} = 280 nm) with the grating at second order. The t = 20 min spectrum shows a slight increase of the BE emission and appearance of a new and more intense band peaked at ∼425 nm. The 425 nm emission band is attributed to DTS within the bandgap of ZnS, including those that are associated with Cu and Br. In the t = 30 min sample, the BE peak decreased to be about the same intensity as the t = 0 min sample while the redder peak due to DTS red-shifted to 440 nm and almost doubled in intensity. The t = 40 min sample is similar to that of t = 30 min sample except the BE peak slightly increased and the DTS peak decreased and red-shifted further to about 458 nm. The t = 60 min sample continued the trend with DTS emission red-shifting to close to 463 nm.

After 2 h, the BE peak increased in intensity to be slightly greater than the DTS emission peak, which decreased and red-shifted to around 468 nm. After 3 h, the 350 nm band increased further in intensity, while the DTS PL band decreased substantially. The NCs initially show mainly BE emission that continues to grow over time, first slowly and then quickly, while the DTS emission to the red is weak initially and then grows in intensity in the first 30 min and subsequently decreases to becoming almost unnoticeable in 3 h. The DTS PL emission also red-shifts during this time. The fast increase in BE emission intensity after 40 min is likely due to improved crystallinity and reduced density of trap states of the sample with reaction time. The disappearance of DTS emission is associated with the "self-purification" of the NCs, where Cu and Br are forced out of the NCs with longer reaction times.[2]

The PL emission spectra of undoped ZnS NCs in the range of 300 to 550 nm are shown with reaction progress in Figure 5. After 1 h of reaction at 280 °C the PL emission exhibited a small BE emission band peaked at 350 nm with an intensity of 27 and a slightly smaller DTS emission band peaked around 440 nm. After 2 h, the BE emission peak intensity more than doubled in intensity, and the DTS emission was no longer observed. The reaction ended after 3.5 h, after which time the BE emission climbed to an intensity of 95. The fwhm was ∼50 nm. After the NCs were washed, the BE emission decreased to an intensity of 15. This decrease is associated with cleaning off capping ligands and opening

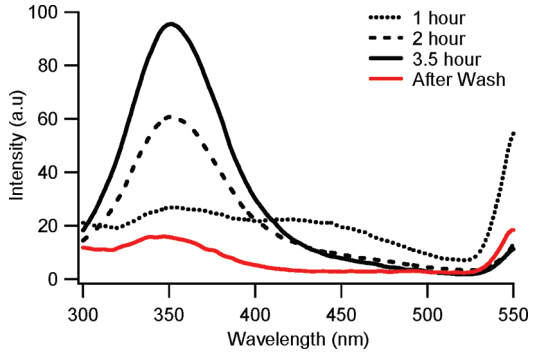

Figure 5. The PL emission with λ_{ex} = 280 nm spectra of undoped ZnS NCs crude reaction mix after 1, 2, and 3.5 h, and the cleaned ZnS NCs after 3.5 h reaction time.

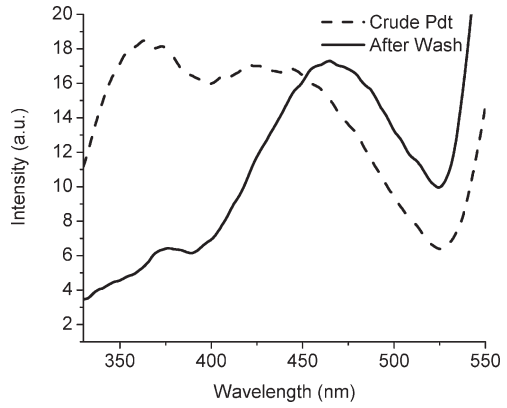

Figure 6. The PL emission spectra with λ_{ex} = 280 nm of undoped ZnS NCs crude product and after cleaning.

up trap states that quench BE emission, as will be discussed in section 4.1.

The PL spectra of undoped ZnS NCs after 1 h reaction time at 280 °C before and after cleaning are shown in Figure 6. These undoped ZnS NCs differ from those presented in Figure 5 because of their shorter reaction time, but their preparation is the same as that of the codoped ZnS:Cu,Br NCs presented in Figure 7. The PL emission spectrum of the crude reaction mix before being cleaned exhibits a near-BE emission band peaked at 362 nm with a full width at half maximum (fwhm) of 50 nm and an intensity of 18 and a DTS emission band peaked at 438 nm with a greater fwhm of 65 nm and a similar intensity. The PL emission spectrum of the undoped ZnS NCs after cleaning exhibits only a small peak with an intensity of 6 from the BE emission at ~350 nm, and a DTS emission peak with a similar intensity to the crude product, but red-shifted 39 to 477 nm.

The PL emission spectra of the crude reaction mix and the cleaned ZnS:Cu,Br (0.8%) NCs are shown in Figure 7. The PL emission of the crude product has a DTS emission band peaked at 450 nm with an intensity of 78 and a small BE emission shoulder at 350 nm. The PL emission peak of the cleaned NCs, compared to the crude product, exhibits a slight red-shift of 7−457 nm and a great leap in intensity to 183 with a fwhm of 75 nm.

The PL emission spectra of undoped cleaned ZnS, ZnS:Cu, ZnS:Br, and ZnS:Cu,Br NCs are shown in Figure 8. The undoped ZnS NCs exhibits a DTS emission band peaked at 467 nm with

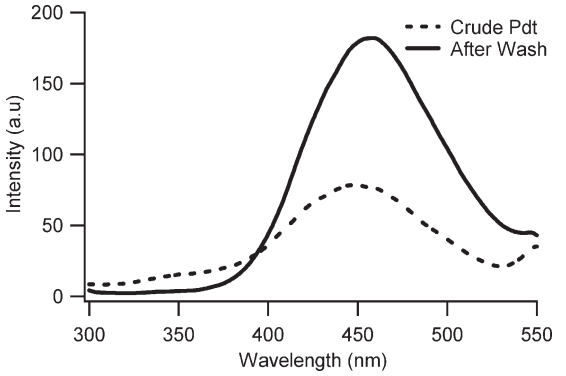

Figure 7. The PL emission spectra with λ_{ex} = 280 nm of ZnS:Cu,Br (0.8%) NCs crude product and after cleaning.

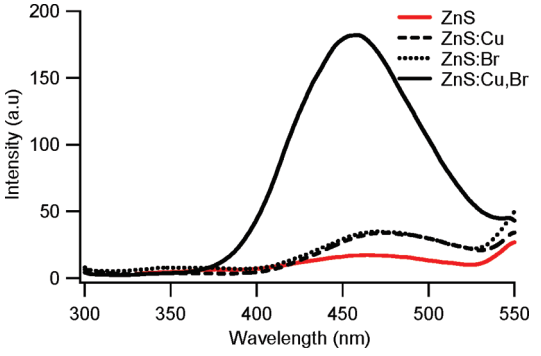

Figure 8. The PL emission spectra with λ_{ex} = 280 nm of undoped ZnS, ZnS:Cu (0.8%), ZnS:Br, and ZnS:Cu,Br (0.8%) NCs after cleaning.

an intensity of 17. The ZnS:Cu and ZnS:Br NCs both have DTS emission bands peaked around 480 nm with similar intensities around 35. The ZnS:Cu,Br has PL emission that is significantly more intense with a peak position at 460 nm, an intensity of 182, and a fwhm of 85 nm.

3.3. Time-Resolved PL Studies. To gain a more complete understanding of the electronic energy transfer process in the undoped and doped NCs, time-resolved PL measurements were conducted. As the undoped samples had significantly less PL than the doped samples, it required characterization by fixing the start of the detector gate 20 ns after the laser pulse and starting with a 50 ns width, widening the gate to collect for longer times out to 20 000 ns. The doped samples allowed the decay spectra to be collected by fixing the gate width and moving the collection gate delay with respect to the pump pulse. The resulting time-resolved PL spectra for the three types of representative samples were reported as a composite in Figure 9. The figures corresponding to the undoped sample are labeled "1", the ZnS:Cu is labeled as "2", and the ZnS:Cu,Br as "3". Three methods for displaying the decay spectra were presented; as a contour plot of wavelength (nm) versus time delay (ns) versus intensity labeled as "a", wavelength versus intensity labeled "b", and the resulting lifetime spectra from the global fitting plotted as initial intensity versus wavelength labeled "c". While ZnS was collected by varying the delay width with a fixed start gate, the data presented in panel 1a has been processed to emulate a wavelength versus delay spectra for ease of comparison to 2a and 3a. It has, however, been presented in panel 1b and 1c as it was collected and fit with the inset labels in Figure 1b referring to gate width (ns). A further noteworthy

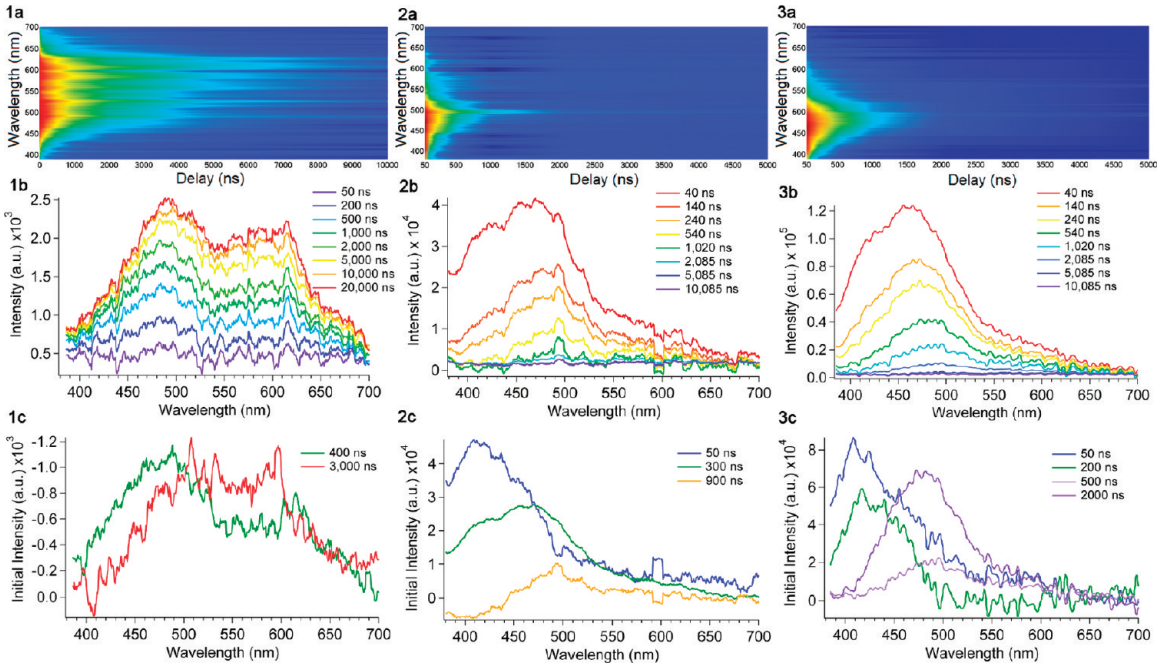

Figure 9. Time-resolved PL spectra of (1) undoped ZnS NCs, (2) ZnS:Cu NCs, and (3) codoped ZnS:Cu,Br NCs in panels a and b, and with corresponding globally fit data in panel c.

distinction is the initial intensity in panel 1c that has negative values corresponding to the inverted fitting resulting from the collection method.

The undoped ZnS sample contour plot (1a) and decay spectra (1b) showed a broad emission spectra as detected with this method spanning from 400 to 650 nm, most of which decayed before 1 μs while a much longer component persisted out to 10 μs. The ZnS:Cu sample had a λ_{max} of 470 nm but lacked much emission beyond 550 nm that lasted for much more than a few hundred nanosecond. It did, however, have a component which extended 2 μs at 500 nm. The rest of the emission from 380 to 500 nm decayed before 500 ns as can be seen in 2a and 2b. The ZnS:Cu,Br sample had a very similar emission profile as the ZnS:Cu with a λ_{max} of 470 nm and it was clearly comparable between panels 2b and 3b. However, it did demonstrate longer decay components, which lasted up to 5 μs at the peak maximum.

The fitting of the time-resolved PL spectra was done using global fitting routines described previously.[54,55] The PL intensity as a function of wavelength and time, $I_f(\lambda, \Delta t)$, could be described by the relationship in eq 1; where I_f, detected for a given gate width Δt and wavelength λ, $I_{f,t>20\ ns}(\lambda)$, is the total luminescence for times longer than 20 ns, $I_1(\lambda)$ is the luminescence that decays with time constant τ_1 as a function of λ, and the "..." indicates further exponential functions required for multiexponential decay fitting.[54,55]

$$I_f(\lambda, \Delta t) = I_{f,t>20ns}(\lambda)[1 - I_1(\lambda)e^{-\Delta t/\tau}...] \quad (1)$$

Estimation of the error mainly associated with the experimental measurement, which is the largest source of error in this characterization, was determined by individually fitting seven single wavelength decays across the spectral feature. The standard deviation of the single wavelength fits was determined to be within 30−40% of the reported number. However, it is expected that the single wavelength fitting results will induce more error than the global fitting routines due to both the exponential prefactor and time constant being averaged out, as both of these variables can contribute to fitting error. We can therefore state that the error is less than 40% and more likely closer to 30%. However, at longer time delays we can estimate the error to be slightly larger due to the lower contribution of that lifetime component to the overall decay spectrum. However, it is not likely to fall outside of our estimates.

Global fitting of the time-resolved PL spectra of the pristine ZnS NCs required a double exponential fit with time constants of 400 ± 100 and 3000 ± 1000 ns. The lifetime spectra (1c) showed that the two components were distributed nearly equally over the emission spectrum with the blue components decaying somewhat faster than the red ones.

The ZnS:Cu sample required three decay components to describe the decay spectra, which were 50 ± 15, 300 ± 80, and 900 ± 300 ns. The 50 ns component had a large initial intensity comparatively and was primarily in the blue wavelengths. The 300 ns component was about half the initial intensity and described components mostly near 480 nm but did have a sideband of 420 nm, and it also extended over the entire decay spectrum. The longest lifetime exhibited some negative values at 400 nm which were due to noise, but did have a max of 500 nm and was required to describe a component extending ±50 nm from the max.

Finally, the ZnS:Cu,Br was fit with four life times, which were 50 ± 15, 200 ± 70, 500 ± 150, and 2,000 ± 500 ns. The fast component had a very similar lifetime spectrum as the Cu-doped sample as it described blue components with a λ_{max} of 410 nm; however, the initial intensity did not dominate the spectrum as it had in that sample. The 200 ns component was required to describe very similar wavelengths to the 50 ns component but was not required to describe wavelengths past 500 nm. Compared to the Cu-doped 300 ns component, it appeared that the maximum contribution of 480 nm was eliminated while the sideband of 420 nm remained. There was a new substantial lifetime component in the codoped sample with the lifetime of 500 ns that described

dx.doi.org/10.1021/jp202734n |J. Phys. Chem. C 2011, 115, 14559–14570

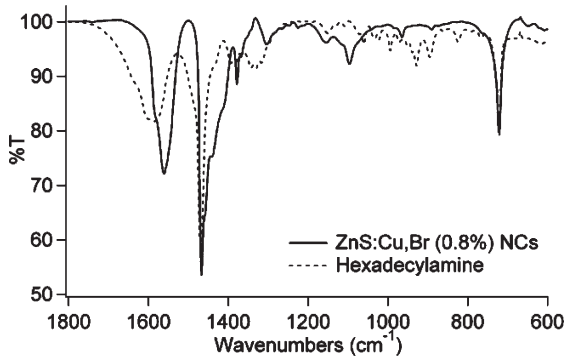

Figure 10. FTIR spectra of ZnS:Cu,Br (0.8%) NCs thin film on NaCl plate (black line) and hexadecylamine in KBr pellet (gray line).

wavelengths from 420 to 600 nm with a maximum of 490 nm. The initial intensity from this component was comparable to that of the fast component if the noise is not considered. The same wavelength components described by the 500 ns lifetime were mirrored in a final lifetime with a time constant of 2 ± 0.5 μs. The data were also fit with three lifetimes, which was not sufficient. The three-lifetime fit is included in the Supporting Information, as well as the residuals from the three and four lifetime fit, which are reduced significantly enough to warrant the addition of the fourth lifetime.

3.4. FTIR Surface Characterization. After the NCs were thoroughly cleaned, identification of the capping ligand was performed using FTIR spectroscopy. The spectrum of ZnS:Cu,Br (0.8%) compared to that of a primary amine, hexadecylamine, is shown in Figure 10. The most indicative peaks in the NCs spectrum corresponded to NH_2 scissoring (1559 cm^{-1}), CH_2 scissoring (1467 cm^{-1}), CN stretching (1097 cm^{-1}), NH_2 out-of-plane bending (shoulder 765 cm^{-1}), and CH_2 rocking (731 cm^{-1}).[56] Therefore, the resulting spectrum corresponded to a primary amine. Subsequently, the identity of this species was verified against hexadecylamine, an analogous aliphatic primary amine. It was thereby concluded that the capping ligand was in fact of the same family as hexadecylamine, unintentionally added along with the TOA since primary amines are known contaminants in the 98% purity TOA. As approximately 7.3 g (9 mL) of TOA was used in the reaction, as much as 146 mg octylamine (~1 mmol) was added as well. It is reasonable to expect that the primary amine would be the most stable on the NC surface over the other compounds in solution, most being tertiary and having large steric interference.

The other potential competitive interaction for surface sites would be with the acids used in the synthesis including stearic and oleic acid (totaling 0.64 mmol). However, at high temperatures it is known that primary and secondary amines will react with acids to form amides. It is reasonable to conclude that because there were no acid-functionalized capping ligands observed in the FTIR, these compounds were in effect removed from the system by this mechanism.

4. DISCUSSION

4.1. Surface Effect on PL. Due to their large surface-to-volume ratio, the surface of NCs plays a critical role in determining their electronic and optical properties by introducing trap states within the bandgap. The NCs synthesized by the method described above had to be cleaned immediately after the synthesis to preserve their PL properties, or their trap state emission would decrease significantly and permanently. After the NCs were cleaned, their PL became stabilized. We propose that in the crude reaction mix, there was a reactive species that binds to the naked S sites on the surface of the NCs and quenches the DTS luminescence in an irreversible process. It is likely due to the excess alkanethiol in solution, which has been previously shown to significantly quench the PL of CdSe NCs.[57] As the process appeared to be irreversible, it is possible that the alkanethiol binds covalently through a disulfide bond. Upon cleaning the NCs immediately after the synthesis, this species was removed from solution and the PL was stabilized.

Cleaning the undoped NCs had the effect of quenching the bandedge emission, as shown in Figure 5, and red-shifting the DTS emission, as shown in Figure 6. Since the capping ligand was found to be a primary amine through FTIR analysis (Figure 10), as discussed in section 3.4, it is expected to bind to the Zn sites on the surface of the NCs and leave S dangling bonds responsible for quenching BE emission.[58,59] The red-shift originated from washing away some of the amine capping ligands from the Zn sites, exposing Zn dangling bonds that create trap states similar to those calculated by Bryant in the case of uncapped Cd on the surface of CdS NCs.[59] For the undoped NCs, this red-shift associated with cleaning the NCs was 39 nm (~0.2 eV), as can be observed in Figure 6, compared to a red-shift of 7 nm (~0.05 eV) in the codoped ZnS:Cu,Br NCs. The much smaller red-shift observed in the ZnS:Cu,Br NCs can be explained by the fact that Br adds an electron trap into the bandgap of ZnS ~0.25 eV below the conduction band.[69] Since the energy level of this electron trap is very close to that of the Zn dangling bond, the red-shift is much smaller for the codoped NCs than for the undoped NCs. The relevant energy levels are shown in Figure 11 and the implications will be further discussed in the following sections.

Upon cleaning the codoped NCs, a significant increase in PL (>2 ×) was also observed (Figure 7). This increase was not observed in the case of undoped ZnS (Figure 6), and observed to a lesser extent in Cu- or Br- singly doped NCs. This large increase in PL of the codoped NCs upon cleaning is likely due to the removal of the excess alkanethiol. Upon its removal, the nonradiative pathways associated with it are reduced and more efficient emission may occur due to the codoping of Br and Cu.

4.2. Local Structure of Br. The excellent fit of Br on an S site of ZnS confirmed its incorporation into the ZnS lattice. Its unusually small amplitude though is more difficult to explain. Here we need to point out that one other sample that had a reasonable Br fluorescence signal had no significant EXAFS peaks in *r*-space (<25% of the first peak in Figure 2). Consequently, in that sample, most of the Br was not incorporated into ZnS but was in some disordered structure, likely loosely bound to the surface of the NCs. This corresponds to a small fraction of the Br originally introduced during synthesis. There is no peak corresponding to a Br−Zn bond. We can explain the reduced amplitude for the data shown in Figure 2 as follows. If a fraction of the Br (from 25 to 50%) was incorporated into the ZnS NCs, it would have quite well-defined peaks for various shells of neighbors, but with the overall amplitude significantly lower (by the fraction of Br incorporated). If the remaining fraction (50−75%) of the Br were a highly disordered structure similar to that on the one sample that had essentially no EXAFS, then one can understand the low amplitude, as only the Br with an ordered environment would contribute. This would also explain why the amplitude ratio remained close to 1:3 as the overall amplitude varied. Also, if the small fraction of disordered Br that remains varied from

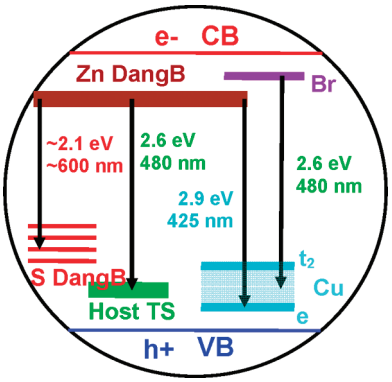

Figure 11. Proposed energy diagram for undoped, Cu-doped, and Cu and Br codoped ZnS NCs. The red emission at 600 nm (2.1 eV) and green emission at 480 nm (2.6 eV) in the undoped ZnS NCs are illustrated as originating from shallow traps below the conduction band (~0.5 eV) created by Zn dangling bonds. The associated hole traps for these transitions are DTS created by S dangling bonds, and shallower trap states within the ZnS host (originating from either S dangling bonds or Zn vacancies). In the Cu-doped ZnS NCs, the DTS created by S dangling bonds are blocked. A blue emission at 425 nm (2.9 eV) is observed, which is attributed to emission from Zn dangling bonds to the hole trap created by the Cu *e* state. The green emission band previously assigned is still present. In the Cu and Br codoped ZnS NCs, the same emissions due to Cu-doped ZnS NCs are observed with an additional component at the same peak position as the blue emission at 480 nm (2.6 eV) but with a different lifetime and increased intensity. This transition is assigned to be D−A luminescence between the Br electron trap (~0.3 eV below the conduction band (CB)) and Cu hole trap (0.3−1.3 eV above the valence band (VB)).

sample to sample (perhaps as a result of the cleaning procedure), it would explain the variation in overall amplitude.

Thus it is concluded that some of the Br is incorporated into the ZnS structure with Br on the S site. Less local disorder about such sites compared to Cu in ZnS can be explained by the fact that CuBr is also a zincblende structure, in contrast to CuS, which is a layered structure. The Br may add to the ZnS lattice without creating as much disorder in the structure compared to when Cu is added. The effect of Cu increasing the disorder in the structure around Br is a good indication that the Br is close to the Cu, which is in alignment with the change in PL that occurs upon codoping. Cu EXAFS (not included) on a few of the same Br samples have a similar first Cu−S peak to earlier ZnS:Cu NCs studies,[25] but more Cu K-edge data for a range of samples are needed to compare the Cu environments.

4.3. PL of Undoped ZnS. The undoped ZnS NCs had very weak PL (Figure 8), which indicates that there is a high prevalence of nonradiative pathways likely due to surface DTS within the bandgap. The time-resolved PL data revealed two emission bands, as shown in Figure 9 (1a and 1b), one centered around 480 nm, referred to as the green band, and another centered around 600 nm, referred to as the red band. The global data fit reveals that the green band decays with a 400 ns lifetime, while the red band decays with a much longer lifetime of 3 μs. The shorter lifetime is attributed to emission from shallow trap states created by Zn dangling bonds to DTS created by either S dangling bonds or Zn vacancies (V_{Zn}) located about 0.6 eV above the valence BE. Figure 11 shows the relevant energy levels involved in the PL emission bands observed. S dangling bonds are expected to create a distribution of trap states, shallow and deep, above the valence band.[58−61] The V_{Zn} is known to form a hole acceptor state that is about 1 eV above the bandgap in bulk ZnS and responsible for its self-activated (SA) luminescence.[46,48,60,62] It is reasonable to believe V_{Zn} would be present due to the great excess of S compared to Zn (6:1) that was used during the synthesis.

The red band is attributed to emission from the Zn dangling bonds to DTS created by S dangling bonds. Uncapped S dangling bonds are expected to create an array of trap states from very shallow traps to DTS above the valence band.[58,59] This assignment is also based on the long PL decay lifetime of 3 μs, which is consistent with the trend that deeper traps, specifically surface localized DTS, tend to decay with a longer lifetime.[63−65]

4.4. Effect of Cu-Doping on PL of ZnS NCs. Upon doping the ZnS NCs with Cu, the overall static PL intensity increased slightly while the spectral profile was similar to that of the undoped sample. However, the PL decay profile based on time-resolved measurement is altered upon Cu doping, indicating that Cu is incorporated into the NCs. This is also confirmed by EXAFS measurement. The lack of spectral shift upon doping with Cu is unique to this study compared to most previous studies, where a clear red-shift is observed with increasing Cu concentration.[8,23,25,30] In our previous work,[25] it was found that the emission could be tuned between 440 and 487 nm by varying the amount of Cu between 0% to 3%. A key difference in the previous system was that it was aqueous and to achieve efficient PL, an excess of Zn over S was added (2:1). Therefore, the PL emission in the undoped ZnS NCs was likely due to S vacancies, which create an electron trap below the conduction band of the host.[28,60] The excess Zn also serves to stabilize the NCs by aiding in shell formation for more efficient capping, thus the S dangling bonds that create nonradiative pathways in an aqueous system were eliminated.[25,66] Without the presence of either V_{Zn} or S dangling bonds, known to create trap states above the valence band of the host, there were no hole acceptor states in the undoped ZnS NCs. Doping with Cu added a new acceptor state above the valence band where there was previously none. This new state was then responsible for red-shifting the PL upon Cu doping.

By contrast, the undoped ZnS NCs presented in this work were synthesized with an excess of S over Zn (6:1) that lead to the creation of an acceptor state above the valence band created by either V_{Zn} or S dangling bonds. Since these intrinsic defects in the undoped NCs create hole acceptor energy levels within the bandgap with energy very similar to those created by doping with Cu (Figure 11), addition of Cu causes no red-shift.

Since there is no shift in PL emission upon doping with Cu, it is more difficult to conclude whether the Cu states are directly involved in the radiative pathway. In the time-resolved PL spectra shown in Figure 9 (2a and 2b), there is one broad band centered around 480 nm, similar to the green band observed in the undoped sample. The disappearance of the red band with Cu-doping is noted and explained by Cu acting as a hole trap that prevents further migration of the hole into those DTS.

The similar static PL emission spectra of the undoped and Cu-doped samples, in conjunction with the disappearance of the red band for the Cu-doped sample in the time-resolved PL data, suggest three possible explanations of the role of Cu in the PL emission process. First, the Cu-dopant could be a hole acceptor that captures the hole that is created upon excitation. Radiative emission from the electron trapped on the Zn dangling bond to the hole trapped on Cu would result in emission directly involving Cu. The second possibility is that the Cu facilitates hole transport, but is not directly involved in the transition. In

this explanation, the Cu hole-acceptor state enables the hole to become trapped more efficiently in the same trap state as is present in the undoped ZnS host NCs (either a V_{Zn} or a S dangling bond). The emission would then result from the same transitions within the host NCs, but facilitated by the Cu-dopant trap state. The third possibility is a combination of the two effects.

Our data best supports the third possibility. The time-resolved PL of the two samples shows the prominent distinction of the disappearance of the red emission band upon Cu-doping explained earlier, which could support either the direct or indirect role of the Cu hole acceptor blocking hole migration to DTS. The remaining decay lifetime of the green band in the undoped sample is 400 ns, which has a similar shape and decay lifetime as the green band in the Cu-doped sample that decays with a lifetime of 300 ns. The similar position of these bands, accompanied by the faster decay and more intense emission in the Cu-doped sample, leads to the conclusion that they both describe the same transition in the ZnS host in the undoped and Cu-doped sample, but the latter is facilitated by the Cu hole acceptor. The hole can transfer to Cu, then to a trap state in the host. With the hole transfer facilitation provided by Cu, the hole transfer rate is increased, which results in the slightly shorter lifetime, greater efficiency, and hence increased emission intensity.

The data fitting of the Cu-doped sample also reveals a new faster decay feature, the blue emission band centered around 425 nm with a 50 ns lifetime. Since this emission band is not similar to any emission band in the undoped sample, it is attributed to emission directly to the Cu hole acceptor. Since the electron originates from the trap state 0.5 eV below the conduction band created by Zn dangling bond and the emission band is centered around 425 nm (2.9 eV), that places the hole acceptor 0.3 eV above the valence band. The energy levels created by Cu in the bandgap from the tetrahedral splitting of the Cu d orbitals into the *e* and *t* energy bands have been reported to be about 0.3 and 1.3 eV above the valence band.[47,67−70] The 425 nm emission is therefore assigned to transition between the Zn dangling bond electron trap state to the Cu *e* state hole trap ∼0.3 eV above the valence band. The reason that the other Cu state is not involved could be due to poor overlap between wave functions of the *t* Cu state and the state associated with the Zn dangling bond, which leads to low PL intensity.

The final lifetime component of the Cu-doped sample, which is centered around 500 nm and has a lifetime of 900 ns, can be attributed to a transition either related directly to Cu or within the host. Assuming that the Zn dangling bonds make up the electron trap, the hole trap for this transition is ∼0.7 eV above the valence band. It is not observed in the undoped ZnS NCs, which could either mean that it was not present, or that it was of too low an emission intensity to be observed. Without any further evidence, we cannot conclude whether this emission directly involves Cu or is instead due to the host ZnS; either possibility is reasonable.

The effect of doping the ZnS NCs with Cu is that of blocking the hole from migrating to DTS, as evidenced by the disappearance of the red emission band. The emission involves Cu directly as the hole acceptor as well as indirectly as the hole facilitator to increase ZnS host emission. Although Cu plays a role in the emission, the PL of the ZnS:Cu NCs is still rather low and hence dominated by nonradiative trap states within the bandgap.

4.5. Effect of Br and Cu Codoping on PL of ZnS NCs. Br was introduced into the ZnS NCs as a codopant with Cu to improve the PL properties. As a general strategy, codoping has been used to synthesize bulk ZnS:Cu phosphors, usually using Cl.[22,28,33,45−49] The Cu precursor originally investigated was copper acetate, which was changed to copper chloride to add chloride that could potentially codope the NCs, as used in commercially available bulk ZnS:Cu,Cl.[9,68] There was no observable improvement from this change. Addition of excess F was also attempted, which was the codopant leading to the greatest enhancement of PL emission in the work of Manzoor.[28] Tetra-*n*-butylammonium fluoride was used as a fluoride source, as it is soluble in organic media. Addition of this salt showed no change in the PL emission properties of the ZnS:Cu NCs either. Finally, codoping using Br was attempted by adding TOAB, which resulted in the desired result, being a drastic increase in PL (>5×) as shown in Figure 8.

Upon codoping the ZnS NCs with both Cu and Br, aside from the great increase in PL, the spectra was not shifted nor did it change shape in any substantial way. The lack of spectral change with addition of a codopant is typical.[22,28] The time-resolved PL of the ZnS:Cu,Br NCs is also similar to that of the ZnS:Cu NCs with green emission band around 480 nm, a blue emission shoulder around 425 nm, and no red emission band, as shown in Figure 8 (2 and 3).

The time-resolved PL data of the ZnS:Cu,Br NCs can be fit using three or four lifetimes, with four providing a better fit, as explained earlier. The three lifetime fit looked similar to that of the ZnS:Cu NCs and would suggest that the Br^- was not directly involved in the PL transition but rather simply facilitated charge transfer and reduced nonradiative pathways. Since this three-lifetime fit was not as good as the four lifetime fit, this possible model will not be discussed further, and the following discussion will be based on a four-lifetime fit.

The four-lifetime fit shown in Figure 9 (3c) shows that the blue band centered around 425 nm with a 50 ns lifetime is preserved from the ZnS:Cu NC sample, and is thus attributed to emission from the Zn dangling bond state to the Cu *e* state. There is another blue band also centered around 425 nm with a 200 ns lifetime. This lifetime is similar to that of the green band in the ZnS:Cu. For the green band in the Cu-doped NCs, the peak was centered around 480 nm, but there was also a clearly defined shoulder around 425 nm. The blue band in the codoped sample can be attributed to the same transition as that in the Cu-doped NCs due to its similar lifetime and resemblance to the blue shoulder that was present in the Cu-doped NCs spectrum. The PL near 480 nm is weaker, and the related lifetime is reduced for the codoped sample compared to that of the Cu-doped sample. The reason for the apparent disappearance could be the much more intense emission peak that grew in at the same wavelength and then buried this peak.

The emission around 480 nm with a lifetime of 500 ns is at a similar position as the green band present in the undoped and Cu-doped NCs, but has a longer lifetime. To determine whether this band could be due to emission from the Br electron trap to the Cu hole trap, the energy levels are considered. The energy level created by Br was determined to be ∼0.2−0.3 eV below the conduction band, while the Cu acceptor energy level is expected to create states in the range of 0.3−1.3 eV above the valence band, as shown in Figure 11. If emission is considered to take place between these states, the energy of this transition would be ∼2.6 eV, or ∼475 nm. This matches the wavelength of the green emission band with a lifetime of 500 ns. Since emission at this wavelength is present even before codoping, there is more than one possible assignment for states involved in this transition. We assign it to the D−A transition from Br to Cu for the following reasons. First, the static PL emission intensity is increased by

more than 5 times when both Cu and Br are present in the sample together, while doping either one independently does not show such an effect. Second, the 480 nm emission band is exactly at the location that would be predicted for this transition and is a very wide band, corresponding to the energy states created by the tetrahedral split of Cu^+ *d* orbitals.[47,67−70] Third, this type of D−A transition between halogen and Cu codopants has been observed in bulk ZnS:Cu,halogen (or Al^{3+}).[46−49]

The emission band centered around 480 nm with a lifetime of 2 μs is another new feature of the codoped NCs. Because its position and shape are similar to that of the 500 ns peak that is assigned to the transition between Br and Cu, it is attributed to transitions that also involve Br and Cu, possibly a dipole forbidden triplet to singlet state transition because of the very long lifetime.

The synergistic effect of codoping the ZnS NCs with both Cu and Br is clearly evidenced by the great increase in PL emission in the codoped NCs compared to the undoped, Cu-, or Br-doped NCs. The Cu and Br dopants are likely located near each other substituting for Zn and S ions, respectfully, as evidenced by EXAFS. Their combined presence enables efficient D−A pair luminescence that competes with nonradiative relaxation pathways that dominate the PL in undoped or singly doped ZnS NCs.

5. CONCLUSION

Fluorescent Cu,Br-doped ZnS NCs were synthesized via the hot-injection method. This is the first demonstration, to our best knowledge, of using Br as a coactivator in an organic solvent system to successfully improve PL in Cu-doped ZnS NCs. The addition of Cu alone to the NCs did not significantly change the PL emission characteristics of the NCs. When Br was doped into the NCs in addition to Cu, a significant increase in PL emission was observed. The local structures of both Cu and Br have been studied using EXAFS and indicate that Br is incorporated into the ZnS lattice and near to Cu. The enhancement of PL is synergistic as the codoping results in PL much stronger than the simple sum of PL from single doping using Cu and Br separately. On the basis of static and time-resolved PL results, the enhanced PL due to codoping is attributed to radiative recombination of electrons in Br-associated trap states and holes in Cu-associated trap states within the bandgap of ZnS. This synergistically enhanced PL from codoping is not only interesting fundamentally but also opens the door for important technological applications of codoped semiconductor nanomaterials.

■ ASSOCIATED CONTENT

Supporting Information. An example of the Br K-edge k-space data for the ZnS:Cu,Br sample containing 0.8% Cu; ZnS:Cu,Br NCs time-resolved PL data globally fit using three lifetimes; residuals from the three- and four-lifetime fit of the time-resolved PL of ZnS:Cu,Br NCs; and PL decay traces of ZnS:Cu and ZnS:Cu,Br NCs at 470, 490, and 530 nm, along with the fitting functions used to describe the decays. This material is available free of charge via the Internet at http://pubs.acs.org.

■ AUTHOR INFORMATION

Corresponding Author
*E-mail: zhang@ucsc.edu.

■ ACKNOWLEDGMENT

This project is funded by the U.S. Department of Energy (DE-FG02-07ER46388-A002). We would like to thank Jim Lewis for taking time-resolved PL data and helping with the analysis. We are grateful for the use of the HRTEM facilities at the National Center of Electron Microscopy, Lawrence Berkeley National Laboratory, which is supported by the U.S. Department of Energy under Contract Number DE-AC02-05CH11231 and Dr. Chenyou Song for his assistance. We would like to thank Rebecca Newhouse for insightful discussion and Yutaro Sano for assistance in some of the synthesis. The EXAFS experiments were carried out at the Stanford Synchrotron Radiation Lightsource, a Directorate of SLAC National Accelerator Laboratory and an Office of Science User Facility operated for the U.S. Department of Energy Office of Science by Stanford University.

■ REFERENCES

(1) Bhargava, R. N.; Gallagher, D.; Hong, X.; Nurmikko, A. Optical properties of manganese-doped nanocrystals of ZnS. *Phys. Rev. Lett.* **1994**, *72*, 416.
(2) Erwin, S. C.; Zu, L.; Haftel, M. I.; Efros, A. L.; Kennedy, T. A.; Norris, D. J. Doping semiconductor nanocrystals. *Nature* **2005**, *436*, 91.
(3) Norris, D. J.; Efros, A. L.; Erwin, S. C. Doped nanocrystals. *Science* **2008**, *319*, 1776.
(4) Bhargava, R. N. Doped nanocrystalline materials—Physics and applications. *J. Lumin.* **1996**, *70*, 85–94.
(5) Bussian, D. A.; Crooker, S. A.; Yin, M.; Brynda, M.; Efros, A. L.; Klimov, V. I. Tunable magnetic exchange interactions in manganese-doped inverted core−shell ZnSe−CdSe nanocrystals. *Nat. Mater.* **2009**, *8*, 35.
(6) Chen, D.; Viswanatha, R.; Ong, G. L.; Xie, R.; Balasubramaninan, M.; Peng, X. Temperature dependence of "elementary processes" in doping semiconductor nanocrystals. *J. Am. Chem. Soc.* **2009**, *131*, 9333.
(7) Yu, J. H.; Liu, X.; Kweon, K. E.; Joo, J.; Park, J.; Ko, K.-T.; Lee, D. W.; Shen, S.; Tivakornsasithorn, K.; Son, J. S.; Park, J.-H.; Kim, Y.-W.; Hwang, G. S.; Dobrowolska, M.; Furdyna, J. K.; Hyeon, T. Giant Zeeman splitting in nucleation-controlled doped CdSe:Mn^{2+} quantum nanoribbons. *Nat. Mater.* **2010**, *9*, 47.
(8) Karan, N. S.; Sarma, D. D.; Kadam, R. M.; Pradhan, N. Doping transition metal (Mn or Cu) ions in semiconductor nanocrystals. *J. Phys. Chem. Lett.* **2010**, *1*, 2863.
(9) Srivastava, B. B.; Jana, S.; Pradhan, N. Doping Cu in semiconductor nanocrystals: Some old and some new physical insights. *J. Am. Chem. Soc.* **2011**, *133*, 1007.
(10) Chen, W.; Zhang, J. Z.; Joly, A. G. Optical properties and potential applications of doped semiconductor nanoparticles. *J. Nanosci. Nanotechnol.* **2004**, *4*, 919–947.
(11) Wang, F.; Liu, X. Upconversion multicolor fine-tuning: Visible to near-infrared emission from lanthanide-doped $NaYF_4$ nanoparticles. *J. Am. Chem. Soc.* **2008**, *130*, 5642–5643.
(12) Meulenberg, R. W.; van Buuren, T.; Hanif, K. M.; Willey, T. M.; Strouse, G. F.; Terminello, L. J. Structure and composition of Cu-doped CdSe nanocrystals using soft X-ray absorption spectroscopy. *Nano Lett.* **2004**, *4*, 2277–2285.
(13) Colvin, V. L.; Schlamp, M. C.; Alivisatos, A. P. Light-emitting diodes made from cadmium selenide nanocrystals and a semiconducting polymer. *Nature* **1994**, *370*, 354–357.
(14) Manzoor, K.; Vadera, S. R.; Kumar, N.; Kutty, T. R. N. Multicolor electroluminescent devices using doped ZnS nanocrystals. *Appl. Phys. Lett.* **2009**, *84*, 284–286.
(15) Wood, V.; Halpert, J. E.; Panzer, M. J.; Bawendi, M. G.; Bulovic, V. Alternating Current Driven Electroluminescence from ZnSe/ZnS:Mn/ZnS Nanocrystals. *Nano Lett.* **2009**, *9*, 2367–2371.
(16) Yang, H.; Holloway, P. H.; Ratna, B. B. Photoluminescent and electroluminescent properties of Mn-doped ZnS nanocrystals. *J. Appl. Phys.* **2003**, *93*, 586.

(17) Rath, A. K.; Bhaumik, S.; Pal, A. J. Mn-doped nanocrystals in light-emitting diodes: Energy-transfer to obtain electroluminescence from quantum dots. *Appl. Phys. Lett.* **2010**, 97.

(18) Tan, Z.; Zhang, F.; Zhu, T.; Xu, J.; Wang, A. Y.; Dixon, J. D.; Li, L.; Zhang, Q.; Mohney, S. E.; Ruzyllo, J. Bright and color-saturated emission from blue light-emitting diodes based on solution-processed colloidal nanocrystal quantum dots. *Nano Lett.* **2007**, *7*, 3803.

(19) Coe, S.; Woo, W.-K.; Bawendi, M.; Bulovic, V. Electroluminescence from single monolayers of nanocrystals in molecular organic devices. *Nature* **2002**, *420*, 800.

(20) Sun, Q.; Wang, Y. A.; Li, L. S.; Wang, D.; Zhu, T.; Xu, J.; Yang, C.; Li, Y. Bright, multicoloured light-emitting diodes based on quantum dots. *Nat. Photonics* **2007**, *1*, 717.

(21) Dabbousi, B. O.; Bawendi, M. G.; Onitsuka, O.; Rubner, M. F. Electroluminescence from CdSe quantum dot/polymer composites. *Appl. Phys. Lett.* **1995**, *66*, 1316.

(22) Shionoya, S., Yen, W. M., Eds. *Phosphor Handbook*; CRC Press LLC: Boca Raton, FL, 1999.

(23) Ehlert, O.; Osvet, A.; Batentschuk, M.; Winnacker, A.; Nann, T. Synthesis and spectroscopic investigations of Cu- and Pb-doped colloidal ZnS nanocrystals. *J. Phys. Chem. B* **2006**, *110*, 23175.

(24) Jian, W.; Zhuang, J.; Zhang, D.; Dai, J.; Yang, W.; Bai, Y. Synthesis of highly luminescent and photostable ZnS: Ag nanocrystals under microwave irradiation. *Mater. Chem. Phys.* **2006**, *99*, 494–497.

(25) Corrado, C.; Jiang, Y.; Oba, F.; Kozina, M.; Bridges, F.; Zhang, J. Z. Synthesis, structural, and optical properties of stable ZnS:Cu,Cl nanocrystals. *J. Phys. Chem. A* **2009**, *113*, 3830.

(26) Hoshina, T.; Kawai, H. Luminescence excitation spectra and their exciton structures of ZnS Phosphors. I. Mn, (Cu, Al), (Ag, Al) and (Au, Al) Doped Phosphors. *Jpn. J. Appl. Phys.* **1980**, *19*, 267–277.

(27) Khosravi, A. A.; Kundu, M.; Jatwa, L.; Deshpande, S. K.; Bhagwat, U. A.; Sastry, M.; Kulkarni, S. K. Green luminescence from copper doped zinc sulphide quantum particles. *Appl. Phys. Lett.* **1995**, *67*, 2702.

(28) Manzoor, K.; Vadera, S. R.; Kumar, N.; Kutty, T. R. N. Synthesis and photoluminescent properties of ZnS nanocrystals doped with copper and halogen. *Mater. Chem. Phys.* **2003**, *82*, 718.

(29) Mukherjee, P.; Shade, C. M.; Yingling, A. M.; Lamont, D. N.; Waldeck, D. H.; Petoud, S. Lanthanide sensitization in II−VI semiconductor materials: A case study with terbium(III) and europium(III) in zinc sulfide nanoparticles *J. Phys. Chem. A* **2011**

(30) Corrado, C.; Hawker, M.; Livingston, G.; Medling, S.; Bridges, F.; Zhang, J. Z. Enhanced Cu emission in ZnS:Cu, Cl/ZnS core−shell nanocrystals. *Nanoscale* **2010**, *2*, 1213–1221.

(31) Ma, L.; Chen, W. ZnS:Cu, Co water-soluble afterglow nanoparticles: Synthesis, luminescence and potential applications. *Nanotechnology* **2010**, *21*, 385604.

(32) Chen, W.; Joly, A. G.; Malm, J.-O.; Bovin, J.-O. Upconversion luminescence of Eu^{3+} and Mn^{2+} in ZnS:Mn^{2+}, Eu^{3+} codoped nanoparticles. *J. Appl. Phys.* **2004**, *95*, 667.

(33) Reilly, K. T.; Gingerich, R. G. W. Process for producing electroluminescent phosphors of improved brightness. U.S. Patent 4,859,361, 1989.

(34) Wu, C. C.; Chun, J. K. M.; Burrows, P. E.; Sturm, J. C.; Thompson, M. E.; Forrest, S. R.; Register, R. A. Poly(p-phenylene vinylene)/tris(8 hydroxy) quinoline aluminum heterostructure light emitting diode. *Appl. Phys. Lett.* **1995**, *66*, 653.

(35) Wang, M.; Sun, L.; Fu, X.; Liao, C.; Yan, C. Synthesis and optical properties of ZnS:Cu(II) nanoparticles. *Solid State Commun.* **2000**, *115*, 493–496.

(36) Klausch, A.; Althues, H.; Schrage, C.; Simon, P.; Szatkowski, A.; Bredol, M.; Adam, D.; Kaskel, S. Preparation of luminescent ZnS:Cu nanoparticles for the functionalization of transparent acrylate polymers. *J. Lumin.* **2010**, *130*, 692.

(37) Porambo, M. W.; Marsh, A. L. Synthesis and photoluminescent properties of doped ZnS nanocrystals capped by poly(vinylpyrrolidone). *Opt. Mater.* **2009**, *31*, 1631.

(38) Xu, S. J.; Chua, S. J.; Liu, B.; Gan, L. M.; Chew, C. H.; Xu, G. Q. Luminescence characteristics of impurities-activated ZnS nanocrystals prepared in microemulsion with hydrothermal treatment. *Appl. Phys. Lett.* **1998**, *73*, 478.

(39) Huang, J.; Yang, Y.; Xue, S.; Yang, B.; Liu, S.; Shen, J. Photoluminescence and electroluminescence of ZnS:Cu nanocrystals in polymeric networks. *Appl. Phys. Lett.* **1997**, *70*, 2335.

(40) Katsuhiko, H.; Yoshio, I.; Kei, M. Etching effect on AC powder EL phosphor brightness and maintenance. *J. Electrochem. Soc.* **1982**, *129*, 2059–2062.

(41) Katsuhiko, H.; Haruki, K.; Bunjiro, T. AC powder electroluminescence maintenance Improvement. *Journal of The Electrochemical Society* **1983**, *130*, 2448–2452.

(42) Chander, H.; Shanker, V.; Haranath, D.; Dudeja, S.; Sharma, P. Characterization of ZnS:Cu, Br electroluminescent phosphor prepared by new route. *Mater. Res. Bull.* **2003**, *38*, 279.

(43) Nien, Y. T.; Chen, I. G. Raman scattering and electroluminescence of ZnS:Cu, Cl phosphor powder. *Appl. Phys. Lett.* **2006**, *89*, 261906.

(44) Nien, Y.-T.; Chen, I.-G.; Hwang, C.-S.; Chu, S.-Y. Copper concentration dependence of structure, morphology and optical properties of ZnS:Cu,Cl phosphor powder. *J. Phys. Chem. Solids* **2006**, *69*, 366.

(45) Stanley, J.; Jiang, Y.; Bridges, F.; Carter, S. A.; Ruhlen, L. Degradation and rejuvenation studies of AC electroluminescent ZnS: Cu, Cl phosphors. *J. Phys.: Condens. Matter* **2010**, *22*, 055301.

(46) Prener, J. S.; Williams, F. E. Self activation and self coactivation in zinc sulfide phosphors. *J. Chem. Phys.* **1956**, *25*, 361.

(47) Suzuki, A.; Shionoya, S. Mechanism of the green-copper luminescence in ZnS crystals. I. Direct evidence for the pair emission mechanism. *J. Phys. Soc. Jpn.* **1971**, 31.

(48) Bowers, R.; Melamed, N. T. Luminescent centers in ZnS:Cu:Cl phosphors. *Phys. Rev.* **1955**, *99*, 1781.

(49) Williams, F. Donor−acceptor pairs in semiconductors. *Phys. Status Solidi B* **1968**, *25*, 493–512.

(50) Hirabayashi, K.; Kozawaguchi, H.; Tsujiyama, B. AC powder electroluminescence maintenance improvement. *J. Electrochem. Soc.* **1983**, *130*, 2448.

(51) Rehr, J. J.; Booth, C. H.; Bridges, F.; Zabinsky, S. I. X-ray-absorption fine structure in embedded atoms. *Phys. Rev. B* **1994**, *49*, 12347.

(52) Li, G.; Bridges, F.; Brown, G. S. Multielectron X-ray photoexcitation observations in X-ray-absorption fine-structure background. *Phys. Rev. Lett.* **1992**, *68*, 1609–1612.

(53) Ankudinov, A. L.; Ravel, B.; Rehr, J. J.; Conradson, S. D. Real-space multiple-scattering calculation and interpretation of X-ray-absorption near-edge structure. *Phys. Rev. B* **1998**, *58*, 7565.

(54) Hug, S. J.; Lewis, J. W.; Einterz, C. M.; Thorgeirsson, T. E.; Kliger, D. S. Nanosecond photolysis of rhodopsin: Evidence for a new blue-shifted intermediate. *Biochemistry* **1990**, *29*, 1475–1485.

(55) Szundi, I.; Lewis, J. W.; Kliger, D. S. Deriving reaction mechanisms from kinetic spectroscopy. Application to late rhodopsin intermediates. *Biophys. J.* **1997**, *73*, 688.

(56) Segal, L.; Eggerton, F. V. Infrared spectra of aliphatic normal mono-amines and alpha−omega diamines. *Appl. Spectrosc.* **1961**, *15*, 112–116.

(57) Green, M. The nature of quantum dot capping ligands. *J. Mater. Chem.* **2010**, *20*, 5797.

(58) Choi, S.-H.; An, K.; Kim, E.-G.; Yu, J. H.; Kim, J. H.; Hyeon, T. Simple and generalized synthesis of semiconducting metal sulfide nanocrystals. *Adv. Funct. Mater.* **2009**, *19*, 1645.

(59) Bryant, G. W. Surface states on semiconductor nanocrystals: The effects of unpassivated dangling bonds. *J. Comput. Theor. Nanosci.* **2009**, *6*, 1262–1271.

(60) Wageh, S.; Ling, Z. S.; Xu-Rong, X. Growth and optical properties of colloidal ZnS nanoparticles. *J. Cryst. Growth* **2003**, *255*, 332.

(61) Califano, M.; Franceschetti, A.; Zunger, A. Temperature dependence of excitonic radiative decay in CdSe quantum dots: The role of surface hole traps. *Nano Lett* **2005**, *5*, 2360–2364.

(62) Kasai, P. H.; Otomo, Y. Electron paramagnetic resonance studies of the ZnS A and B centers. *J. Chem. Phys.* **1962**, *37*, 1263.
(63) Zhang, J. Z. Ultrafast studies of electron dynamics in semiconductor and metal colloidal nanoparticles: Effects of size and surface. *Acc. Chem. Res.* **1997**, *30*, 423.
(64) Bawendi, M. G.; Carroll, P. J.; Wilson, W. L.; Brus, L. E. Luminescence properties of CdSe quantum crystallites: Resonance between interior and surface localized states. *J. Chem. Phys.* **1992**, *96*, 946.
(65) Zhang, J.; Zhang, X.; Zhang, J. Y. Size-dependent time-resolved photoluminescence of colloidal CdSe nanocrystals. *J. Phys. Chem. C* **2009**, *113*, 9512.
(66) Wu, F.; Zhang, J. Z.; Kho, R.; Mehra, R. K. Radiative and nonradiative lifetimes of band edge states and deep trap states of CdS nanoparticles determined by time-correlated single photon counting. *Chem. Phys. Lett.* **2000**, *330*, 237.
(67) Hagston, W. E. Molecular orbital theory for Cu^{2+} in tetrahedral co-ordination. *J. Phys. C: Solid State Phys.* **1968**, *1*, 810.
(68) Shionoya, S.; Kobayashi, Y.; Koda, T. Polarization of the green-copper luminescence in hexagonal ZnS single crystal. *J. Phys. Soc. Jpn.* **1965**, 20.
(69) Apple, E. F.; Prener, J. S. On the infrared emission in ZnS:Cu—Effect of sulfur pressure and aluminum. *J. Phys. Chem. Solids* **1960**, *13*, 81.
(70) Peka, P.; Schulz, H. J. Empirical one-electron model of optical transitions in Cu-doped ZnS and CdS. *Phys. B: Condens. Matter* **1994**, *193*, 57–65.